Highly excited core resonances in photoionization of Fe XVII: Implications for plasma opacities

Sultana N. Nahar,[1,*] Anil K. Pradhan,[1] Guo-Xin Chen,[2] and Werner Eissner[3]
[1]*Department of Astronomy, The Ohio State University, Columbus, Ohio 43210, USA*
[2]*ITAMP, Harvard-Smithsonian Center for Astrophysics, 60 Garden Street, Cambridge, Massachusetts 02138, USA*
[3]*Institut für Theoretische Physik, Teilinstitut 1, D-70550 Stuttgart, Germany*
(Received 31 January 2011; published 20 May 2011)

A comprehensive study of high-accuracy photoionization cross sections is carried out using the relativistic Breit-Pauli *R*-matrix (BPRM) method for ($h\nu$ + Fe XVII → Fe XVIII + e). Owing to its importance in high-temperature plasmas, the calculations cover a large energy range, particularly the myriad photoexcitation-of-core (PEC) resonances including the $n = 3$ levels not heretofore considered. The calculations employ a close-coupling wave-function expansion of 60 levels of the core ion Fe XVIII ranging over a wide energy range of nearly 900 eV between the $n = 2$ and $n = 3$ levels. Strong-coupling effects due to dipole transition arrays $2p^5 \rightarrow 2p^4(3s,3d)$ manifest themselves as large PEC resonances throughout this range and enhance the effective photoionization cross sections orders of magnitude above the background. Comparisons with the erstwhile Opacity Project (OP) and other previous calculations show that the currently available cross sections considerably underestimate the bound-free cross sections. A level-identification scheme is used for spectroscopic designation of the 454 bound fine structure levels of Fe XVII, with $n \leqslant 10$, $l \leqslant 9$, and $0 \leqslant J \leqslant 8$ of even and odd parities, obtained using the *ab initio* BPRM method (compared to 181 LS bound states in the OP work). The calculated energies are compared with those available from the National Institute for Standards and Technology database, which lists 63 levels with very good agreement. Level-specific photoionization cross sections are computed for all levels. In addition, partial cross sections for leaving the core ion Fe XVII in the ground state are also obtained. These results should be relevant to modeling of astrophysical and laboratory plasma sources requiring (i) photoionization rates, (ii) extensive nonlocal-thermodynamic-equilibrium models, (iii) total unified electron-ion recombination rates including radiative and dielectronic recombination, and (iv) plasma opacities. We particularly examine PEC and non-PEC resonance strengths and emphasize their expanded role to incorporate inner-shell excitations for improved opacities, as shown by the computed monochromatic opacity of Fe XVII.

DOI: 10.1103/PhysRevA.83.053417 PACS number(s): 32.80.Fb, 96.60.Jw, 52.70.−m

I. INTRODUCTION

High-precision studies of photoionization of atoms in a large number of excited levels are of interest in several areas. Derivative quantities such as laboratory and astrophysical plasma opacities [1–4], spectral models of photoionization-dominated sources such as active galactic nuclei [5], nonlocal-thermodynamic-equilibrium (non-LTE) models of stellar atmospheres [6], and total electron-ion recombination rates [7], depend on the accuracy of the underlying treatment of photoionization for the entire atom (ion) at all energies where it is abundant under specific plasma conditions.

There have been a number of theoretical calculations to produce large amounts of data for practical applications, in particular under the Opacity Project (OP) [3] and the Iron Project (IP) [8], but they are usually limited in terms of accuracy owing to computational constraints and in terms of detailed examination of the photoabsorption process for excited levels. Furthermore, except for light elements or simple few-electron systems, large-scale calculations do not adequately treat the two most important atomic effects: relativistic fine structure and resonances. Many previous calculations are basically in LS coupling [3], or take account of fine structure through an algebraic transformation rather than through a relativistic calculation per se. The primary reason, of course, is that it is difficult to do so, since the calculations for photoionization of a large number of fine structure levels remains an enormous task. Close-coupling calculations that account for the ubiquitous resonances in photoionization cross sections are mostly done using the *R*-matrix method [9–11]. The extension to include relativistic effects led to the development of the Breit-Pauli *R*-matrix (BPRM) codes [12,13] and to aforementioned work under the Iron Project for relatively simple atomic systems such as He-like and Li-like ions (see, e.g., [14]).

Such large-scale calculations with high precision may be of crucial importance in resolving a major astrophysical problem [15] that is related to plasma opacities [16] and recent studies of solar abundances of common elements such as C, N, O, and Ne. The new abundances are widely discordant with the standard solar abundances by up to 50% [15]. The new abundances are derived from high-resolution spectroscopy and the most advanced three-dimensional (3D) hydrodynamic nonlocal-thermodynamic-equilibrium (NLTE) models. However, such a huge decrease in solar elemental composition is not supported by heliosmological observations of solar oscillations measured with great accuracy [17]. In addition, predictions of solar interior models are also in conflict with the new abundances [18]. Given the inverse relationship between opacity and abundances, it has been suggested that a marginal, but highly significant, increase in mean opacities of about 10%–20% could possibly reconcile the new and the standard solar abundances [19].

Another need for higher-precision opacities arises due to the recent capability of creating stellar interior conditions

*nahar@astronomy.ohio-state.edu

in the laboratory [1]. Inertial confinement fusion (ICF) devices can now produce plasmas in local thermodynamic equilibrium (LTE) at temperatures and densities approaching those at the boundary of the radiative zone and the convection zone (CZ) in the Sun. Measurements have been carried out at the Z-pinch facility at Sandia National Laboratory of monochromatic opacity spectra of iron at $T_e \sim 150$–200 eV and $N_e \sim 10^{22}$–10^{23} cm^{-3}. Fe XVII is the largest contributor to opacity amongst the iron ions prevalent at that temperature and density, from Fe XVI–Fe XIX with ionization fractions 0.0757, 0.302, 0.366, and 0.18, respectively. However, there are marked differences between the Z-pinch observations and theoretically computed opacities [1]. Thus, both astrophysical and laboratory observations require high-precision studies to understand or resolve the discrepancies.

We now note one of the basic atomic physics assumptions made in earlier theoretical calculations of plasma opacities; namely, that resonances are treated as lines, and perturbative treatments are then employed to include continuum contributions. Depending on the temperature and density, most of the opacity could stem from inner-shell excitations in complex atomic species such as iron ions with closed L and M subshells [2,20]. Such a photoexcitation-of-core (PEC) process occurs at high energies above the first ionization threshold. Therefore, it manifests itself as resonances in the bound-free cross sections. The corresponding PEC resonances are large features present at incident photon frequencies corresponding to dipole transitions in the core ion [21,22]. It follows that the major source of opacity in any plasma source, astrophysical or in the laboratory, lies in bound-free resonances in general, heretofore treated mostly as bound-bound transitions or lines, and in PEC resonances in particular. But the approximation of resonant photoionization by lines was made in the OP [2,3] and Opacity at Livermore (OPAL) [4] projects because opacity calculations are extremely intensive and require huge amounts of atomic data for all constituent elements in many excitation and ionization states. Nevertheless, good agreement is found between the two projects for mean opacities over a wide range of temperatures and densities [20] (discussed later). But now, owing to the major problems outlined above, it appears necessary to compute atomic parameters to higher precision to address this issue, albeit on a relatively small scale for individual ions to begin with.

This report presents pilot and prototypical calculations required for revised opacity work. Ne-like Fe XVII is a prime contributor to solar opacity near the convection zone boundary [1], with many PEC features in photoionization cross sections. By carrying out one of the most comprehensive BPRM calculations for photoionization of an atomic system, we have computed and analyzed level-specific fine structure cross sections and the distribution of resonances over a wide energy range encompassing complex atomic structures. In previous studies of photoionization including resonances, Fe XVII was studied mainly in the low-energy region using a small wave-function representation. An R-matrix calculation in LS coupling using a two-state wave-function expansion for the core ion Fe XVIII was carried out under the Opacity Project [23]. A later coupled-channel calculation, aimed at unified electron-ion recombination calculations for (e + Fe XVIII) → Fe XVII, employed the (BPRM) method using a three-level [or three-state close-coupling (3CC)] wave-function expansion by Pradhan *et al.* [24]. The recombination spectrum obtained using 3CC photoionization compared very well with the experimentally observed spectrum in the very-low-energy region. But due to the ion's abundance in high-temperature plasmas, a preliminary calculation using a 60-level expansion for Fe XVIII was initiated by Zhang *et al.* [25]. This initial study on photoionization cross sections focused only on one symmetry: levels with total $J = 0$. But to examine its opacity *in toto*, a much more extensive calculation is necessary. This study is a full-scale photoionization calculation using the large 60-level wave-function expansion for Fe XVIII, with energy levels up to approximately 1 keV. That energy range should account for nearly all of the resonance structures due to L-shell excitation of Fe XVII at temperatures ∼200 eV where it is abundant near the solar CZ; the Planckian blackbody distribution decreases to render the Fe XVII ionization fraction and opacity insignificant beyond $E \sim 1.5$ keV. We especially aim to elucidate PEC resonance features that greatly affect photoionization in the high-energy region.

In this report, we point out other potential applications as well. Since the cross sections are computed up to levels with $n(SLJ) \leqslant 10$, they should be useful for NLTE spectral modeling in the x-ray region. The present work yields accurate energies and spectroscopic identification of the 454 bound levels of Fe XVII computed through *ab initio* calculations. In addition, level-specific partial photoionization cross sections of Fe XVII into the ground state of Fe XVIII are computed, as required for future studies of unified recombination cross sections, including both radiative and dielectronic recombination processes.

II. THEORY

Photoionization calculations have been carried out in the close-coupling (CC) approximation using the R-matrix method as developed under the Opacity Project [2,3] and the Iron Project [8,13]. In the CC approximation the atomic system is represented as the "target" or "core" ion of N electrons interacting with the $(N + 1)$th electron. The $(N + 1)$th electron may be bound in the electron-ion system or in the electron-ion continuum depending on whether its energy is negative or positive. The total wave function Ψ_E of the $(N + 1)$-electron system in $J\pi$ symmetry is an expansion over the eigenfunctions of the target ion, χ_i, in the specific state $S_i L_i (J_i)\pi_i$, coupled with the $(N + 1)$th electron function θ_i:

$$\Psi_E(e + \text{ion}) = A \sum_i \chi_i(\text{ion})\theta_i + \sum_j c_j \Phi_j, \qquad (1)$$

where the sum is over the ground and excited states of the target or the core ion. The $(N + 1)$th electron with kinetic energy k_i^2 corresponds to a channel labeled $S_i L_i (J_i)\pi_i k_i^2 \ell_i (SL(J)\pi)$. The Φ_js are bound channel functions of the $(N + 1)$-electron system that account for the short-range correlation not considered in the first term and the orthogonality between the continuum and the bound-electron orbitals of the target.

The relativistic Hamiltonian in the Breit-Pauli R-matrix (BPRM) approximation is given by

$$H_{N+1}^{\rm BP} = \sum_{i=1}^{N+1}\left\{-\nabla_i^2 - \frac{2Z}{r_i} + \sum_{j>i}^{N+1}\frac{2}{r_{ij}}\right\} + H_{N+1}^{\rm mass} + H_{N+1}^{\rm Dar} + H_{N+1}^{\rm so}. \quad (2)$$

where the last three terms are, respectively, the following three relativistic corrections:

$$H^{\rm mass} = -\frac{\alpha^2}{4}\sum_i p_i^4, \quad \text{the mass correction term,}$$
$$H^{\rm Dar} = \frac{Z\alpha^2}{4}\sum_i \nabla^2\left(\frac{1}{r_i}\right), \quad \text{the Darwin term,} \quad (3)$$
$$H^{\rm so} = Z\alpha^2\sum_i \frac{1}{r_i^3}\mathbf{l_i}\cdot\mathbf{s_i}, \quad \text{the spin-orbit interaction term.}$$

Equations (3) represent the one-body terms of the Breit interaction. Another version of "full" BPRM codes has been developed including the two-body terms, but this is only of importance for forbidden ($E2$, $M1$, $M2$) transitions where two-electron correlations may play an important role [26]. In contrast, plasma opacities *in toto* are determined by strong $E1$ (dipole-allowed and intercombination) transitions considered in this work.

Substitution of $\Psi_E(e+\text{ion})$ in the Schrödinger equation

$$H_{N+1}\Psi_E = E\Psi_E \quad (4)$$

introduces a set of coupled equations that are solved using the R-matrix method. The solution is a continuum wave function Ψ_F for an electron with positive energies ($E > 0$), or a bound state Ψ_B at a negative total energy ($E \leqslant 0$). The complex resonance structures in photoionization cross sections result from channel couplings between the continuum channels that are open ($k_i^2 > 0$) and those that are closed ($k_i^2 < 0$). Resonances occur at electron energies k_i^2 corresponding to autoionizing states belonging to Rydberg series, $S_iL_i\pi_i\nu\ell$ where ν is the effective quantum number, converging to the target threshold S_iL_I.

The first term on the right in Eq. (1) represents both bound states and free (continuum) states of the $(e+\text{ion})$ system. If all channels are closed then the state is bound and is represented by Ψ_B; asymptotically, all channel functions are exponentially decaying. On the other hand, a continuum state corresponds to some channels open and some closed and is referred to as Ψ_F. Asymptotically, the open-channel functions are oscillating, as for a free electron. The transition matrix element for photoionization is

$$\langle\Psi_B||\mathbf{D}||\Psi_F\rangle, \quad (5)$$

where $\mathbf{D} = \sum_i r_i$ is the dipole operator and the sum is over the number of electrons; Ψ_B and Ψ_F are the bound and continuum wave functions, respectively. The transition matrix element can be reduced to the generalized line strength as

$$\mathbf{S} = |\langle\Psi_j||\mathbf{D}_L||\Psi_i\rangle|^2 = \left|\langle\psi_f|\sum_{j=1}^{N+1} r_j|\psi_i\rangle\right|^2, \quad (6)$$

where Ψ_i and Ψ_f are the initial- and final-state wave functions, respectively. The photoionization cross section ($\sigma_{\rm PI}$) is proportional to the generalized line strength as

$$\sigma_{\rm PI} = \frac{4\pi^2}{3c}\frac{1}{g_i}\omega\mathbf{S}, \quad (7)$$

where g is the statistical weight factor of the bound state and ω is the incident photon energy (Ry).

III. COMPUTATIONS

BPRM photoionization cross sections of Fe XVII were computed in the 60CC expansion over the core ion Fe XVIII, and free-electron wave functions with partial waves up to $l \leqslant 12$. The one-electron basis set of orbitals used to construct a configuration-interaction representation of the eigenfunctions of Fe XVIII were obtained from the code SUPERSTRUCTURE [27], which employs a Thomas-Fermi-Dirac-Amaldi central field potential. The choice of the one-electron orbital basis set is not unique; Hartree-Fock orbitals of Slater-type orbitals are also used in R-matrix calculations [9–11]. At sufficiently high densities (i.e., $N_e > 10^{22}$ cm^{-3}), the electronic orbitals may themselves be altered by plasma effects such as Debye screening. However, we do not consider those effects in OP calculations which entail the isolated-atom approximation and the so-called "chemical picture" [2,28] (discussed hereafter).

Table I gives the set of 11 configurations with a filled $1s^2$ shell that was optimized to obtain Fe XVIII core wave functions [25]. It lists the 60 levels included in the 60CC expansion. For a small number of levels the available energy-level data [29] compiled by the National Institute for Standards and Technology (NIST) are found to be in very good agreement with theoretical calculations [25]. One of the main points to note, and which is of considerable significance in the energy distribution of resonances, is the clustering of 60 fine structure levels in the $n = 2$ and $n = 3$ complexes and the large energy gap of ∼50 Ry between them. Although the target energies are quite accurate, some further improvement in the resonance positions is also achieved by replacing the Fe XVIII level energies with observed levels, wherever available [29], during diagonalization of the $(N+1)$-electron Hamiltonian of the $(e+\text{Fe XVIII})$ system.

The second sum in the wave-function expansion given in Eq. (1) is the bound-channel term consisting of selected electronic configurations for the electron-ion system. We include 27 configurations of $(N+1)$-electron bound channels of Fe XVII, specified by a range of minimum and maximum occupancies (listed within parentheses after the orbitals) as: $2s(0–2), 2p(3–6), 3s(0–2), 3p(0–2)$, and $3d(0–2)$. We consider all $SLJ\pi$ symmetries of the electron-ion system formed from the target states coupled with an interacting electron with continuum partial waves $0 \leqslant l \leqslant 12$.

The *ab initio* bound-state energies of the electron-ion system computed by the R-matrix codes in intermediate SLJ coupling are not spectroscopically identified *a priori*. For complex ions it is a highly nontrivial task to assign LS-term and SLJ-level designations. It is particularly difficult for fine structure levels computed in BPRM calculations owing to the near-degeneracy of levels in high-Z or high-z ions, particularly

TABLE I. Energy levels of the target ion Fe XVIII included in the eigenfunction expansion of Fe XVII. Note the large energy gap of ∼47 Ry between the $n = 2$ and $n = 3$ complexes. The target was optimized with a set of 11 configurations with open L shell but closed K shell: $2s^22p^5(1)$, $22p2s^6(2)$, $2s^22p^43s(3)$, $2s^22p^43p(4)$, $2s^22p^43d(5)$, $2s2p^53s(6)$, $2s2p^53p(7)$, $2s2p^53d(8)$, $2p^63s(9)$, $2p^63p(10)$, and $2p^63d(11)$.

i	Configuration	Term	$2J$	E(Ry) Present	i	Configuration	Term	$2J$	E(Ry) Present
		$n = 2$ states			30	$2s^22p^43p$	$^2P^o$	1	61.899
1	$2s^22p^5$	$^2P^o$	3	0.00000	31	$2s^22p^43d$	^4D	5	62.299
2	$2s^22p^5$	$^2P^o$	1	0.93477	32	$2s^22p^43d$	^4D	7	62.311
3	$2s2p^6$	^2S	1	9.70228	33	$2s^22p^43d$	^4D	1	62.906
		$n = 3$ states			34	$2s^22p^43d$	^4D	3	63.050
4	$2s^22p^43s$	^4P	5	56.690	35	$2s^22p^43p$	$^2P^o$	3	62.461
5	$2s^22p^43s$	^2P	3	56.936	36	$2s^22p^43d$	^4F	9	62.535
6	$2s^22p^43s$	^4P	1	57.502	37	$2s^22p^43d$	^2F	7	62.629
7	$2s^22p^43s$	^4P	3	57.572	38	$2s^22p^43p$	$^2P^o$	1	62.686
8	$2s^22p^43s$	^2P	1	57.798	39	$2s^22p^43d$	^4P	1	62.496
9	$2s^22p^43s$	^2D	5	58.000	40	$2s^22p^43d$	^4P	3	62.625
10	$2s^22p^43s$	^2D	3	58.355	41	$2s^22p^43d$	^4F	5	62.985
11	$2s^22p^43p$	$^4P^o$	3	59.209	42	$2s^22p^43d$	^2P	1	63.123
12	$2s^22p^43p$	$^4P^o$	5	59.238	43	$2s^22p^43d$	^4F	3	63.156
13	$2s^22p^43p$	$^4P^o$	1	59.478	44	$2s^22p^43d$	^2F	5	62.698
14	$2s^22p^43p$	$^4D^o$	7	59.525	45	$2s^22p^43d$	^4F	7	63.271
15	$2s^22p^43p$	$^2D^o$	5	59.542	46	$2s^22p^43d$	^2D	3	63.302
16	$2s^22p^43s$	^2S	1	59.916	47	$2s^22p^43d$	^4P	5	62.911
17	$2s^22p^43p$	$^2P^o$	1	59.982	48	$2s^22p^43d$	^2P	3	63.308
18	$2s^22p^43p$	$^4D^o$	3	60.005	49	$2s^22p^43d$	^2D	5	63.390
19	$2s^22p^43p$	$^4D^o$	1	60.012	50	$2s^22p^43d$	^2G	7	63.945
20	$2s^22p^43p$	$^2D^o$	3	60.147	51	$2s^22p^43d$	^2G	9	63.981
21	$2s^22p^43p$	$^4D^o$	5	60.281	52	$2s^22p^43d$	^2S	1	63.919
22	$2s^22p^43p$	$^2P^o$	3	60.320	53	$2s^22p^43d$	^2F	5	64.200
23	$2s^22p^43p$	$^2S^o$	1	60.465	54	$2s^22p^43d$	^2F	7	64.301
24	$2s^22p^43p$	$^4S^o$	3	60.510	55	$2s^22p^43d$	^2P	3	64.138
25	$2s^22p^43p$	$^2F^o$	5	60.851	56	$2s^22p^43d$	^2D	5	64.160
26	$2s^22p^43p$	$^2F^o$	7	61.028	57	$2s^22p^43d$	^2D	3	64.391
27	$2s^22p^43p$	$^2D^o$	3	61.165	58	$2s^22p^43d$	^2P	1	64.464
28	$2s^22p^43p$	$^2D^o$	5	61.272	59	$2s^22p^43d$	^2D	5	65.305
29	$2s^22p^43p$	$^2P^o$	3	61.761	60	$2s^22p^43d$	^2D	3	65.468

for high n and l. The code PRCBPD [30] is employed for level identification, using the information computed by the BPRM codes, as explained in the next section. In addition, the BPRM energies are cross checked against observations and SUPERSTRUCTURE wherever possible. However, we still note that this is one of the most laborious tasks requiring some judgment in the final assignments for levels highly mixed by configuration interactions.

The present calculations cover a large energy range and variations in the distribution of resonance complexes. In the near-threshold region, below $n = 2$ levels, the $\sigma_{\rm PI}$ were resolved on a fine energy mesh, with 4000 energies up to 0.4 Ry above the ionization threshold. However, such fine resolution is computationally prohibitive for all symmetries and levels over the entire range of ∼65 Ry where resonances due to L-shell excitation occur. There are energy regions where the resonances are sparse, as opposed to regions where they are densely clustered. A number of energy meshes are used to ensure that the overall as well as the detailed contributions of resonances to $\sigma_{\rm PI}$ are taken into account. At photoelectron energies above all 60 target thresholds, the $\sigma_{\rm PI}$ are extrapolated as in [31].

IV. RESULTS AND DISCUSSION

The results of Fe XVII are divided into a few subsections below.

A. Fine Structure levels and oscillator strengths of Fe XVII

Present BPRM calculations for fine structure bound levels are intended to form a complete set for most practical applications. As explained in an earlier paper [32], the high-lying excited core states do not form bound states of the electron-ion system, and corresponding channels have insignificant effect on the bound-state energies. This is particularly true of multiply ionized ions, where there are large gaps between the ground complex and the next excited complex of levels; the energy separation increases as zr. The core ion Fe XVIII has an energy gap of ∼47 Ry between the $n = 2$ and $n = 3$ levels (Table I). Although the present study includes both the $n = 2$ and 3 complexes, all bound levels of Fe XVII have the Fe XVIII parent level as the ground level or another $n = 2$ excited level (i.e., $2s^2p^5\ ^2P^o_{1/2,3/2}$, $2s2p^6\ ^2S_{1/2}$).

R-matrix calculations for bound energy levels entail a "search" for zeros of the electron-ion Hamiltonian [8,33],

where the eigenvalues of the $(N+1)$-electron system occur as in Eq. (4). A total of 454 eigenenergies of Fe XVII were found, subject to the choice of $n \leqslant 10$, $0 \leqslant l \leqslant 9$, and $0 \leqslant J \leqslant 8$ of even and odd parities. These levels have been identified spectroscopically using a numerical procedure implemented in the code PRCBPID [30]. It is based on (i) detailed analysis of quantum defects along Rydberg series of levels, (ii) parentage of the core ion states, (iii) fractional or percentage contributions of closed channels which translate into configuration interactions of corresponding bound-electron-ion configurations, and (iv) angular momentum algebra. The level and energies are similar to the 3CC case carried by Zhang *et al.* [25], with some differences because of mixed levels and near-degenerate quantum defects.

For relatively few levels, the present calculated energies of Fe XVII are compared with the observed values available in the NIST compilation [29] in Table II. The overall agreement is very good, ∼0.1% or better, for most levels including those that are highly excited. The number next to the J value in Table II (column 3) is the relative position of the corresponding calculated energy in its own symmetry $J\pi$. As an example, we discuss levels of a particular symmetry, $SLJ : {}^1P^o_1$. In the present work we obtain 35 ${}^1P^o_1$ levels, as opposed to 11 given in the NIST tables; they are compared in Table II. Of those 11 energies, 5 energies agree to ∼0.1% or better. That includes highly excited levels such as $2s^22p^64p\,{}^1P^o_1$, listed as the 19th computed level (column 3). For two other levels, $2s^22p^56d\,{}^1P^o_1$ and $2s^22p^55d\,{}^1P^o_1$, the energies agree to ∼0.2% and 0.3%, respectively. However, the energies of the remaining three levels differ by 1% to 4%. The largest discrepancy is for level $2s^22p^55s\,{}^1P^o_1$. The complete set of 454 energies with spectroscopic designations is available electronically (at the NORAD atomic data website [34]).

We also report that the oscillator strengths for electric dipole transitions among all the bound levels are obtained and are available electronically. The earlier set corresponds to 3CC calculations [35].

B. Photoionization cross sections of Fe XVII

Photoionization cross sections of all 454 bound fine structure levels of Fe XVII are computed and analyzed in a variety of ways, in particular the distribution of resonances that lie in the large energy gap between the $n = 2$ and $n = 3$ complexes. This is a comprehensive set of cross sections computed using the BPRM method, as required for applications such as plasma opacities, synthetic spectral models, and spectral diagnostics of x-ray absorption lines observed from astronomical objects. The BPRM calculations yield about two and a half times as many levels as the previous OP calculations in LS coupling [36], which resulted in 181 LS bound states with $n(SL) \leqslant 10$. Some important characteristic features of the BPRM cross sections are illustrated and discussed below.

1. Photoionization of the ground state

First we consider the ground state of Fe XVII. Figure 1 presents photoionization cross sections $\sigma_{\rm PI}$ of the ground state $2s^22p^6\,{}^1S$. Whereas panel (a) presents the cross section in

TABLE II. Comparison of calculated energies $E_{\rm cal}$ of Fe XVII with the measured values, $E_{\rm obs}$ [29]. i_J indicates position of the calculated level for symmetry J. An asterisk next to a level indicates incomplete set of observed levels for the state. Numbers in brackets represent powers of 10.

Conf	Term	$J : i_J$	$E_{\rm obs}$(Ry)	$E_{\rm cal}$(Ry)
$2s^22p^6$	${}^1S$	0.0 :1	9.2760[1]	9.2925[1]
$2s^22p^53s$	${}^3P^o$	2.0 :1	3.9463[1]	3.9503[1]
$2s^22p^53s$	${}^3P^o$	1.0 :1	3.9323[1]	3.9367[1]
$2s^22p^53s$	${}^3P^o$	0.0 :1	3.8533[1]	3.8560[1]
$2s^22p^53s$	${}^1P^o$	1.0 :2	3.8446[1]	3.8469[1]
$2s^22p^53p$	${}^3S$	1.0 :1	3.7238[1]	3.7284[1]
$2s^22p^53p$	${}^3D$	3.0 :1	3.6863[1]	3.6902[1]
$2s^22p^53p$	${}^3D$	2.0 :1	3.6981[1]	3.7027[1]
$2s^22p^53p$	${}^3D$	1.0 :3	3.6093[1]	3.6114[1]
$2s^22p^53p$	${}^1P$	1.0 :2	3.6780[1]	3.6826[1]
$2s^22p^53p$	${}^3P$	2.0 :2	3.6646[1]	3.6688[1]
$2s^22p^53p$	${}^3P$	1.0 :4	3.5854[1]	3.5880[1]
$2s^22p^53p$	${}^3P$	0.0 :2	3.6244[1]	3.6274[1]
$2s^22p^53p$	${}^1D$	2.0 :3	3.5826[1]	3.5843[1]
$2s^22p^53p$	${}^1S$	0.0 :3	3.4871[1]	3.4828[1]
$2s^22p^53d$	${}^3P^o$	2.0 :2	3.3662[1]	3.3669[1]
$2s^22p^53d$	${}^3P^o$	1.0 :3	3.3778[1]	3.3813[1]
$2s^22p^53d$	${}^3P^o$	0.0 :2	3.3862[1]	3.3895[1]
$2s^22p^53d$	${}^3F^o$	4.0 :1	3.3656[1]	3.3651[1]
$2s^22p^53d$	${}^3F^o$	3.0 :1	3.3599[1]	3.3612[1]
$2s^22p^53d$	${}^3F^o$	2.0 :4	3.2672[1]	3.2670[1]
$2s^22p^53d$	${}^1D^o$	2.0 :3	3.3472[1]	3.3494[1]
$2s^22p^53d$	${}^3D^o$	3.0 :2	3.3393[1]	3.3400[1]
$2s^22p^53d$	${}^3D^o$	2.0 :5	3.2598[1]	3.2601[1]
$2s^22p^53d$	${}^3D^o$	1.0 :4	3.3052[1]	3.3053[1]
$2s^22p^53d$	${}^1F^o$	3.0 :3	3.2563[1]	3.2565[1]
$2s^22p^53d$	${}^1P^o$	1.0 :5	3.2070[1]	3.2049[1]
$2s2p^63p$	${}^3P^o$	1.0*:6	2.7159[1]	2.7122[1]
$2s2p^63p$	${}^1P^o$	1.0 :7	2.6836[1]	2.6809[1]
$2s^22p^54s$	${}^3P^o$	1.0*:8	2.0899[1]	2.0630[1]
$2s^22p^54s$	${}^1P^o$	1.0 :9	2.0014[1]	2.0557[1]
$2s^22p^54d$	${}^3P^o$	1.0*:10	1.8802[1]	1.8750[1]
$2s^22p^54d$	${}^3D^o$	1.0*:11	1.8455[1]	1.8427[1]
$2s^22p^54d$	${}^1P^o$	1.0 :12	1.7590[1]	1.7571[1]
$2s^22p^55s$	${}^3P^o$	1.0*:13	1.2960[1]	1.2739[1]
$2s^22p^55s$	${}^1P^o$	1.0 :14	1.2022[1]	1.2516[1]
$2s^22p^55d$	${}^3P^o$	1.0*:15	1.2022[1]	1.1912[1]
$2s^22p^55d$	${}^3D^o$	1.0*:16	1.1776[1]	1.1749[1]
$2s^22p^55d$	${}^1P^o$	1.0 :17	1.0910[1]	1.0873[1]
$2s2p^64p$	${}^3P^o$	1.0*:18	1.0236[1]	1.0197[1]
$2s2p^64p$	${}^1P^o$	1.0 :19	1.0090[1]	1.0080[1]
$2s^22p^56s$	${}^3P^o$	1.0*:20	8.7776[0]	8.7515[0]
$2s^22p^56d$	${}^3P^o$	1.0*:22	8.1488[0]	8.1405[0]
$2s^22p^56d$	${}^1P^o$	1.0*:24	7.2558[0]	7.2410[0]
$2s^22p^57s$	${}^3P^o$	1.0*:25	6.3810[0]	6.3535[0]
$2s^22p^57d$	${}^3P^o$	1.0*:26	5.9709[0]	6.0260[0]
$2s^22p^57d$	${}^1P^o$	1.0*:29	5.0232[0]	5.0588[0]
$2s^22p^58d$	${}^3P^o$	1.0*:32	4.4582[0]	4.5627[0]
$2s^22p^58d$	${}^1P^o$	1.0*:35	3.6016[0]	3.6512[0]

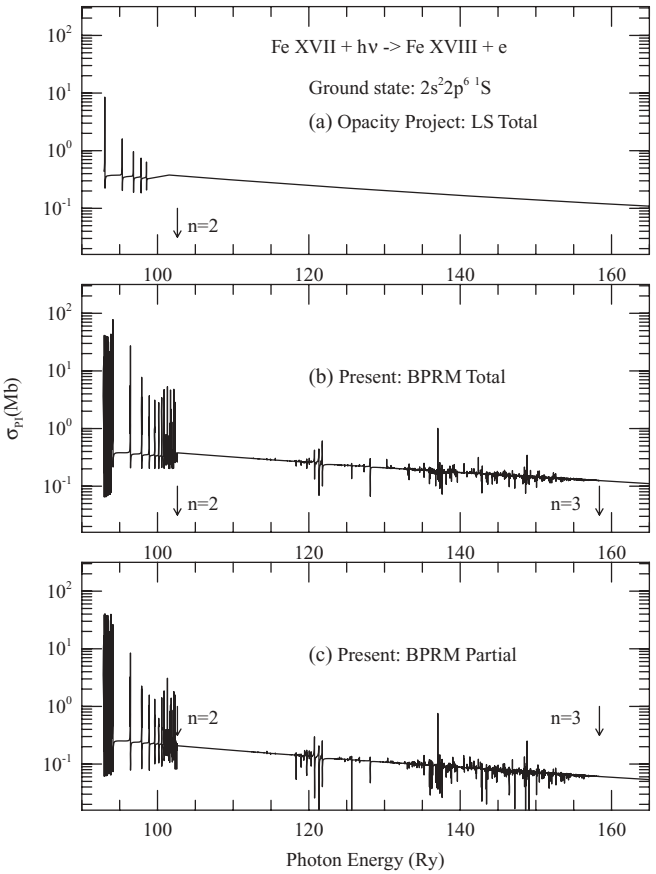

FIG. 1. Photoionization cross sections $\sigma_{\rm PI}$ of the ground level $1s^2 2s^2 2p^6 (^1S_0)$ of Fe XVII: (a) total $\sigma_{\rm PI}$ in LS coupling from the Opacity Project database TOPbase [36], (b) present total $\sigma_{\rm PI}$ in the relativistic BPRM formulation, and (c) present partial $\sigma_{\rm PI}$ with residual ion Fe XVIII in the ground state. Present calculations including relativistic fine structure provide more accurate energies and more highly resolved resonances. The background for the partial cross sections (c) is lower than the total (b) because the channels for leaving the core ion in various excited levels are excluded.

LS coupling under the Opacity Project [23], panels (b) and (c) present $\sigma_{\rm PI}$ from the relativistic BPRM calculations; (b) presents the total cross section and (c) presents the partial cross section for leaving the core ion Fe XVIII in the ground state following photoionization. The earlier total $\sigma_{\rm PI}$ from the two-state R-matrix OP calculation, and the present BPRM using a 60-level expansion are of similar magnitude for the background. However, due to a much larger number of fine structure channels in the BPRM calculation, panel (b) shows many more resonances within the $n = 2$ complex (as also found in the earlier 3CC calculation). Also, a much finer energy mesh in the present work has resolved the resonances more completely. Resolution of resonances in the low-energy region, especially at and near threshold, is crucial for calculating recombination and photoionization rates. The ground state $\sigma_{\rm PI}$ at high energies decreases slowly, showing an insignificant effect due to highly excited $n = 3$ core states in the 60CC calculation, except for introducing small and weak resonance structures.

The partial cross sections in panel (c) correspond to photoionization of Fe XVII leaving the ionized core Fe XVIII only in the ground state. The background is lower than that of the total $\sigma_{\rm PI}$ in (b) because there are no additional contributions from photoionization channels into excited levels. However, the resonance features are the same for the total and partial cross sections until the first-excited state $2s2p^6\,{}^1S_0$ of Fe XVIII.

2. *Photoionization of excited levels*

Although the background ground-state cross sections remain about the same between the 3CC and 60CC calculations, the excited states are considerably more affected. One of the main results of the present BPRM calculations with a large wave-function expansion is that photon absorptions and core excitations to the $n = 3$ levels produce extensive resonance structures, in contrast with earlier calculations. This contradicts the assumption that channels of highly excited core states, especially when an energy gap such as in the present case exists, might be too weakly interacting to produce any significant effect.

Figure 2 presents total photoionization cross sections of excited levels $2s^2 2p^5 3p(^1P^o_1)$ [panels (a) and (b)] and $2s^2 2p^5 3d(^1D^o_2)$ [panels (c) and (d)]. These two levels are

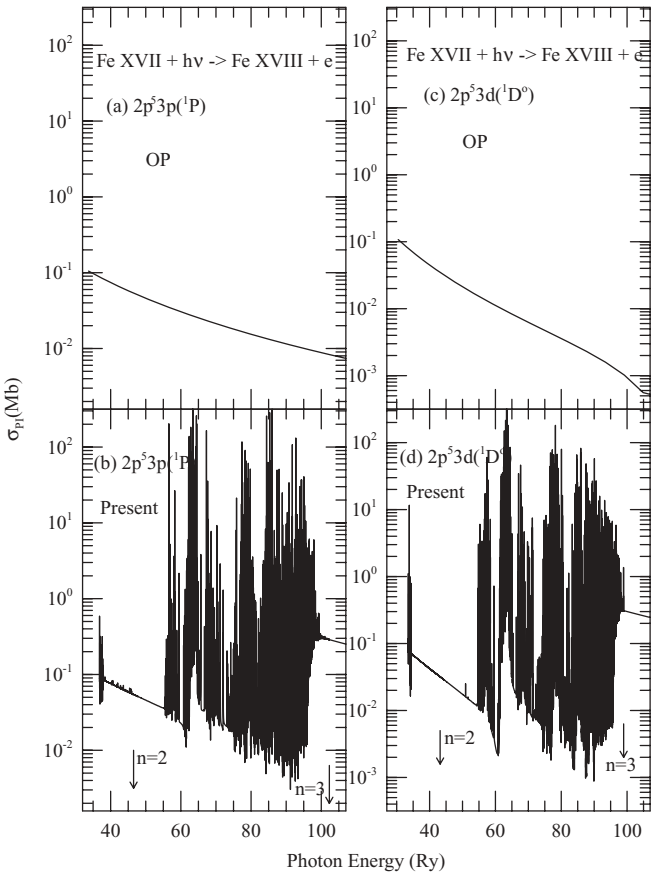

FIG. 2. Comparison of present photoionization cross sections $\sigma_{\rm PI}$ with those from the OP (see [36]) for excited singlet levels (no fine structure): (a), (b) $2p^5 3p\,{}^1P$ and (c), (d) $2p^5 3d(^1D^o)$. In contrast with $\sigma_{\rm PI}$ from OP, the present results demonstrate that, without inclusion of $n = 3$ core levels of Fe XVIII, the cross sections are considerably underestimated throughout most of the energy region of interest in practical applications. Resonances are included as lines in the OP work [3], as in other opacity calculations [4].

chosen because they have a single fine structure component, so their cross sections can be directly compared with the earlier OP results for the LS terms $2s^22p^53p(^1P^o)$ and $2s^22p^53d(^1D^o)$. The top panels (a) and (c) of Fig. 2 present the OP results, and the bottom panels (b) and (d) show results from the present work. Both of these excited levels show resonances due to core excitations to the $n = 2$ and $n = 3$ levels that are not present in the OP results. The features reveal how crucially important the set of resonances belonging to $n = 3$ core thresholds are compared with those of $n = 2$. The resonance peaks are orders-of-magnitude higher than those from the $n = 2$ series. There is only a relatively small gap with a smooth background without resonances between the highest threshold of the $n = 2$ levels and the appearance of the lowest of the $n = 3$ complexes of resonances. While the background is enhanced considerably in the BPRM results by strong resonances, the featureless and slowly decreasing cross sections from the OP miss out all those features and vastly underestimate $\sigma_{\rm PI}$.

Resonances in photoionization cross sections correspond to Rydberg series of autoionizing levels at energies $E_{\rm res} = E_{\rm c}\nu l$, where $E_{\rm c}$ is an excited core threshold and ν_l are the effective quantum number and angular momentum of the interacting electron, respectively. The Rydberg resonances are narrow and lie below the threshold $E_{\rm c}$, approximately at energies given by the simple expression

$$E_{\rm res} = E_{\rm c} - z^2/\nu_l^2. \tag{8}$$

However, strong PEC resonances manifest themselves in the $\sigma_{\rm PI}$ of excited bound levels of the electron-ion system [21,37]. The PEC resonances are wide and occur at energies where the ground state of the core ion undergoes a strong dipole-allowed transition. Among the 60 target or core levels for Fe XVIII, there are 30 such transitions as given in Table III. Hence, in photoionization cross sections of Fe XVII, there are 30 possible PEC resonances, most with overlapping profiles.

Figure 3 presents photoionization cross sections of three highly excited levels of Fe XVII and demonstrably large PEC features; $2s^22p^5nf(^3D_1)$ with $nf = 5f,7f,9f$. Beyond the resonances due to $n = 2$ core levels, the background decreases smoothly for the three levels. However, as the resonances due to $n = 3$ core levels appear, the background rises and the PEC resonances manifest themselves as prominently high and wide structures. These enhancements are related to the radiative decay rates of the dipole-allowed levels. Table III shows that most of the decay rates from $n = 3$ levels are much larger than those from the $n = 2$ levels—by one or two orders of magnitude—and result in stronger resonances. With hundreds of bound levels computed in the present work, the cross sections in the high-energy region from about 57 to 65 Ry is greatly enhanced, mainly by complexes of PEC resonances, which correspond to core excitations via the dipole transitions listed in Table III.

Of particular importance is the characteristic shape of PEC resonances. The resonances encompass an energy range of ~10 Ry or well over 100 eV. The shape is determined by channel-coupling effects. In the case of the simple limit of an isolated resonance it is like the typical Fano profile. However, the PECs are generally affected by strong coupling among many target levels and channels, with a large number of superimposed non-PEC resonances converging to the target levels. The distribution of the continuum or the differential oscillator strength would not be generally reproduced by an isolated-resonance approximation, and requires a coupled-channel calculation.

TABLE III. Dipole-allowed and intercombination $E1$ transitions from the ground level $2s^22p^5(^2P^o_{3/2})$ to excited states of the core ion Fe XVIII and corresponding oscillator strengths (f). These transitions introduce the PEC resonances in photoionization cross sections of Fe XVII. The notation "$a(n)$" means $a \times 10^n$. The level indices correspond to those of Table I. Numbers in brackets represent powers of 10.

Levels	Transition	f(PEC)
1–3	$2s^22p^5(^2P^o_{3/2})$–$2s2p^6(^2S_{1/2})$	5.85[−2]
1–4	$2s^22p^5(^2P^o_{3/2})$–$2s^22p^43s(^4P_{5/2})$	3.57[−3]
1–5	$2s^22p^5(^2P^o_{3/2})$–$2s^22p^43s(^2P_{3/2})$	4.53[−2]
1–6	$2s^22p^5(^2P^o_{3/2})$–$2s^22p^43s(^2P_{1/2})$	1.54[−2]
1–7	$2s^22p^5(^2P^o_{3/2})$–$2s^22p^43s(^4P_{3/2})$	2.12[−2]
1–8	$2s^22p^5(^2P^o_{3/2})$–$2s^22p^43s(^4P_{1/2})$	1.51[−3]
1–9	$2s^22p^5(^2P^o_{3/2})$–$2s^22p^43s(^2D_{5/2})$	3.43[−2]
1–10	$2s^22p^5(^2P^o_{3/2})$–$2s^22p^43s(^2D_{3/2})$	3.87[−4]
1–20	$2s^22p^5(^2P^o_{3/2})$–$2s^22p^43s(^2S_{1/2})$	2.86[−3]
1–31	$2s^22p^5(^2P^o_{3/2})$–$2s^22p^43d(^4D_{5/2})$	2.84[−7]
1–33	$2s^22p^5(^2P^o_{3/2})$–$2s^22p^43d(^4D_{3/2})$	1.43[−4]
1–34	$2s^22p^5(^2P^o_{3/2})$–$2s^22p^43d(^4D_{1/2})$	3.88[−2]
1–37	$2s^22p^5(^2P^o_{3/2})$–$2s^22p^43d(^4P_{1/2})$	8.65[−5]
1–39	$2s^22p^5(^2P^o_{3/2})$–$2s^22p^43d(^4P_{3/2})$	1.31[−1]
1–41	$2s^22p^5(^2P^o_{3/2})$–$2s^22p^43d(^4P_{5/2})$	3.46[−1]
1–42	$2s^22p^5(^2P^o_{3/2})$–$2s^22p^43d(^2P_{1/2})$	4.10[−3]
1–43	$2s^22p^5(^2P^o_{3/2})$–$2s^22p^43d(^2D_{3/2})$	3.58[−2]
1–44	$2s^22p^5(^2P^o_{3/2})$–$2s^22p^43d(^2F_{5/2})$	3.92[−4]
1–46	$2s^22p^5(^2P^o_{3/2})$–$2s^22p^43d(^4F_{3/2})$	9.34[−3]
1–47	$2s^22p^5(^2P^o_{3/2})$–$2s^22p^43d(^4P_{5/2})$	1.38[−2]
1–48	$2s^22p^5(^2P^o_{3/2})$–$2s^22p^43d(^2P_{3/2})$	1.46[−2]
1–49	$2s^22p^5(^2P^o_{3/2})$–$2s^22p^43d(^4F_{5/2})$	2.39[−1]
1–52	$2s^22p^5(^2P^o_{3/2})$–$2s^22p^43d(^2F_{5/2})$	3.37[−2]
1–53	$2s^22p^5(^2P^o_{3/2})$–$2s^22p^43d(^2S_{1/2})$	1.66[−1]
1–55	$2s^22p^5(^2P^o_{3/2})$–$2s^22p^43d(^2P_{3/2})$	3.84[−1]
1–56	$2s^22p^5(^2P^o_{3/2})$–$2s^22p^43d(^2D_{5/2})$	5.08[−1]
1–57	$2s^22p^5(^2P^o_{3/2})$–$2s^22p^43d(^2D_{3/2})$	6.81[−2]
1–58	$2s^22p^5(^2P^o_{3/2})$–$2s^22p^43d(^2P_{1/2})$	4.08[−2]
1–59	$2s^22p^5(^2P^o_{3/2})$–$2s^22p^43d(^2D_{5/2})$	5.24[−2]
1–60	$2s^22p^5(^2P^o_{3/2})$–$2s^22p^43d(^2D_{3/2})$	3.72[−3]

C. Resonance oscillator strengths

A fundamental approximation made in existing opacity calculations is to treat autoionizing resonances as lines. In other words, inner-shell excitations leading to bound-free autoionizing states are treated as bound-bound transitions. The final state may be further coupled perturbatively to a featureless continuum to obtain autoionization widths at a single energy associated with the bound-bound transition. This independent-resonance approximation neglects the intricate coupling effects that are otherwise included via

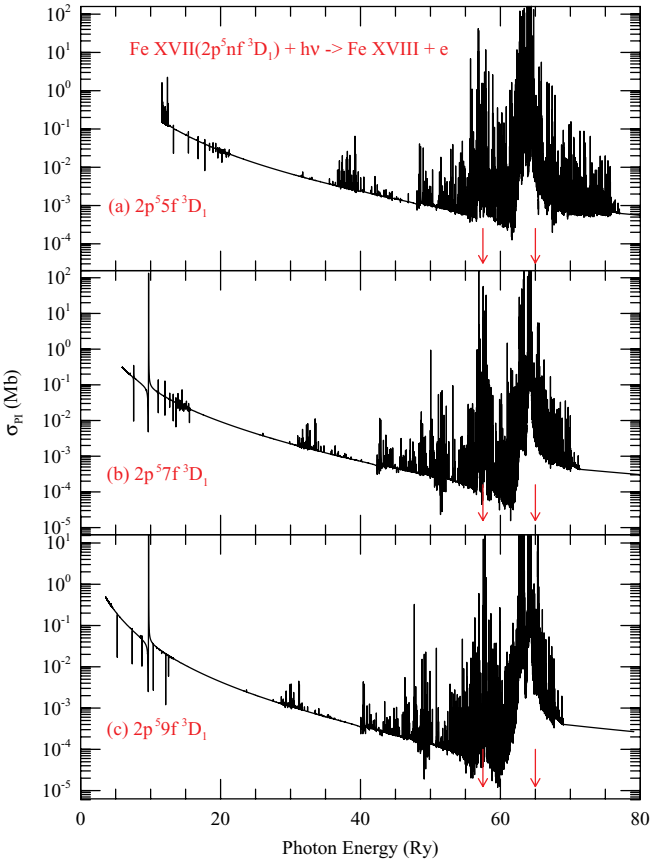

FIG. 3. (Color online) Total photoionization cross section $\sigma_{\rm PI}$ of highly excited levels of Fe XVII: $2s^2 2p^5 nf(^3D_1)$ with $nf = 5f,7f,9f$. The cross sections decrease monotonically at lower energies, but rise considerably when approaching the PEC resonances. The figure shows that the cross sections would be enhanced all throughout the energy range, compared to currently available near-hydrogenic cross sections that decrease much faster as $\sigma_{\rm PI} \sim E^{-3}$. The largest PEC resonances are marked by red arrows. Although only two such PECs are pointed out, the resonance structures and the resulting enhancement represent the combined effect of all PEC resonances in Table III. It may be also be noted that the PEC positions remain the same for all Rydberg levels.

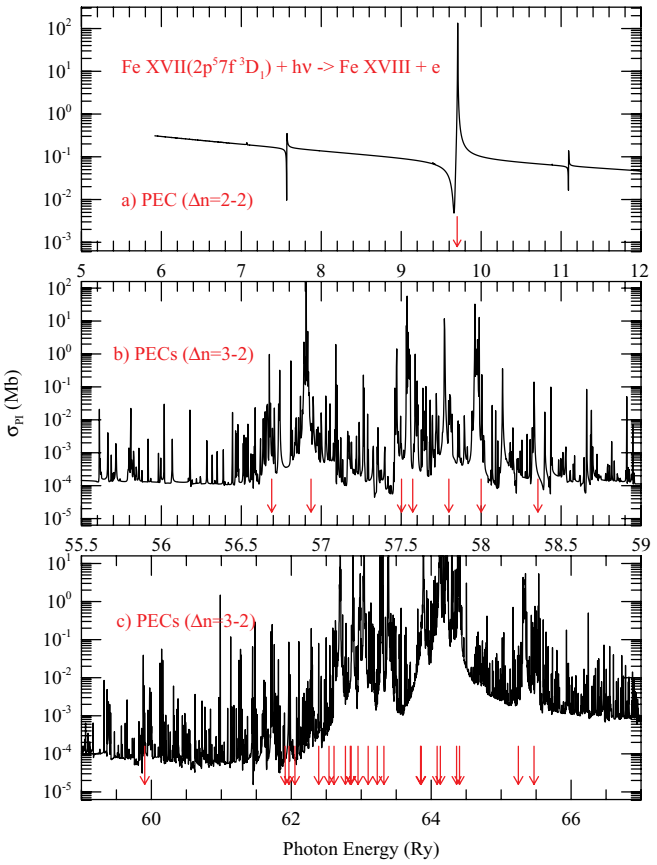

FIG. 4. (Color online) L-shell PEC resonances in photoionization of Fe XVII. The resonances cover all 60 ionization thresholds included in the CC calculation, including all PEC resonances corresponding to $E1$ transitions (dipole-allowed and intercombination) in Table III.

the close-coupling method. Since the main contribution to opacities originates from inner-shell excitations, with final levels as autoionizing states, their impact on opacities bears closer inspection and is briefly discussed below.

In Fig. 4 we examine in some detail one of the cross sections shown in Fig. 3, corresponding to $2s^2 2p^5\ 7f(^3D_1)$. The cross sections are delineated at 24653 energies; the energy intervals are chosen so as to resolve resonance profiles insofar as practical. Positions of all of the PEC resonances due to transitions in Table III are marked in Fig. 4 with red arrows. In addition, there are a large number of non-PEC Rydberg resonances converging to the other excited levels. Whereas the few $\Delta n(2-2)$ resonances in Fig. 4(a) are inconsequential, the myriad $\Delta n(3-2)$ PECs in Figs. 4(b) and 4(c) dominate the distribution of oscillator strength over a large region ~5 to 66 Ry, or >100 eV, due to the L-shell excitation array $2p \rightarrow 3d$. The cumulative resonance (or bound-free continuum) oscillator strength corresponding to Fig. 4 is related to the photoionization cross section (see, e.g., [38]) as

$$f_{\rm r}[(^3D_1 \longrightarrow \epsilon SLJ) :^3(P,D,F)\,(J = 0,1,2)^o] = \left[\frac{1}{4\pi\alpha a_o^2}\right]\int_0^{\epsilon_0} \sigma_{\rm PI}(2s^2 2p^5 7f\ ^3D_1)\,d\epsilon, \qquad (9)$$

where ϵ is the energy relative to the ionization threshold and up to $\epsilon_o \sim 80$ Ry. An integration over the range shown in Fig. 4 yields the partial resonance oscillator strength including all of the PECs and the non-PEC resonances due to coupling of all 60 Fe XVIII levels. The sum over the oscillator strengths corresponding to the 30 PECs gives a total $f_{\rm PEC} = 2.31$. The integrated resonance oscillator strength $f_{\rm r}$ is found to be 4.38. In other words, the 30 PEC resonances involving transitions up to the $n = 3$ levels of the core ion Fe XVIII contribute over half of all the continuum bound-free oscillator strength in photoionization of any excited state of Fe XVII. We note that, without loss of generality, we chose an excited level to demonstrate the quantitative effect of PEC resonances; they manifest themselves in photoionization of most levels.

D. Monochromatic opacities

Opacity calculations are a complex undertaking that requires atomic data for a large number of ions in varying plasma environments [2,4]. One of the main reasons for the large-scale

calculations carried out in the present study is to enable test calculations to benchmark available opacities for Fe ions. To that end, the present BPRM calculations employ similar cutoffs (i.e., $n \leqslant 10$ and $\ell \leqslant n-1$) as the OP work [3]. However, one usually expects only the ground state and low-lying metastable states to be significantly populated. The ionization fractions and level populations are computed using an equation of state, such as the modified Boltzmann-Saha formulation in the "chemical picture" [28], based on the premise that isolated atoms exist, albeit perturbed by the plasma environment [2]. At low densities and temperatures the ion fractions and occupation probabilities of high-lying levels are several orders of magnitude smaller than those for the ground state and metastable levels. But in the high–temperature-density regime of $N_e > 10^{24}$ cm^{-3} and $T_e > 10^6$ K, approaching that in stellar cores, electron-ion recombination rates can be large, and increase rapidly as N_e^2. Even a small population in excited levels would then be susceptible to the resonant enhancements due to PEC resonances, which are currently neglected, and the cross sections for excited levels are taken to be nearly hydrogenic, instead of using the accurate form exemplified in Figs. 2 and 3.

While we have discussed integrated resonance oscillator strengths embedded in bound-free cross sections, there is no direct equivalence or one-to-one correspondence with bound-bound oscillator strengths, as generally computed in opacity calculations. Among the factors that distinguish the two are overlapping profiles and large energy widths of PEC resonances, reflecting the coupling of continua belonging to many target levels and strong dipole moments among them. Owing to the huge scale of data needed, definitive checks can only be made by calculating revised opacities using atomic data, as outlined herein.

A practical problem likely to be encountered is the high energy resolution needed to represent resonance profiles. Whereas scattering cross sections are bounded by the unitarity condition (see, e.g., [22]), no such upper bound exists for individual values of photoionization cross sections. The peak photoionization values may rise arbitrarily high, and numerical integration would tend to be inaccurate as the resonance profile approaches a δ function; the integral is finite but the width is extremely narrow and impractical to resolve. However, the statistical methodology adopted in opacity work is to employ the opacity-sampling technique. Monochromatic opacity spectra are sampled at approximately 10 000 points (see, e.g., [3]), although the atomic data are much more finely resolved. It has been verified that the statistical averages of the most important quantity, the Rosseland Mean Opacity (RMO), do not deviate by more than 1% to 3% even if the atomic cross sections are "sampled" at 10^5 or 10^6 points [2]. Therefore, an energy mesh of ∼30 000 points used in this work, predominantly in the region covered by the high-energy $n = 3$ resonances, which should suffice for accurate opacity calculations.

Figure 5 presents the monochromatic opacity κ (Fe XVII) computed using all of the bound-free data in the present work; 454 photoionization cross sections resolved as discussed above. The calculations are carried out using a newly developed code for high-precision opacities, adapted from the earlier OP work [2] (the OP opacities are available from the online server called OP server at the Ohio Supercomputer Center [36]). The new code also employs a frequency mesh of 10^5 point—an order-of-magnitude finer mesh than OP or OPA—thus obviating some resolution issues in the monochromatic opacity spectra [36]. Essential components of opacity calculations related to bound-bound transitions are retained, as in the OP code: electron-impact and Stark broadening, free-free scattering, and electron-photon interactions in the Rayleigh, Thomson, and Compton scattering limits. However, resonance profiles have not yet been broadened. Whereas bound-bound line shapes are symmetric, the giant PEC-resonance profiles span hundreds of eVs (viz. Figs. 3 and 4) and are asymmetric. Theoretical formulations for broadening of resonances and algorithms are still being developed. However, as mentioned, plasma effects in the chemical picture [28] are included *a posteriori*, and do not affect the accuracy of the

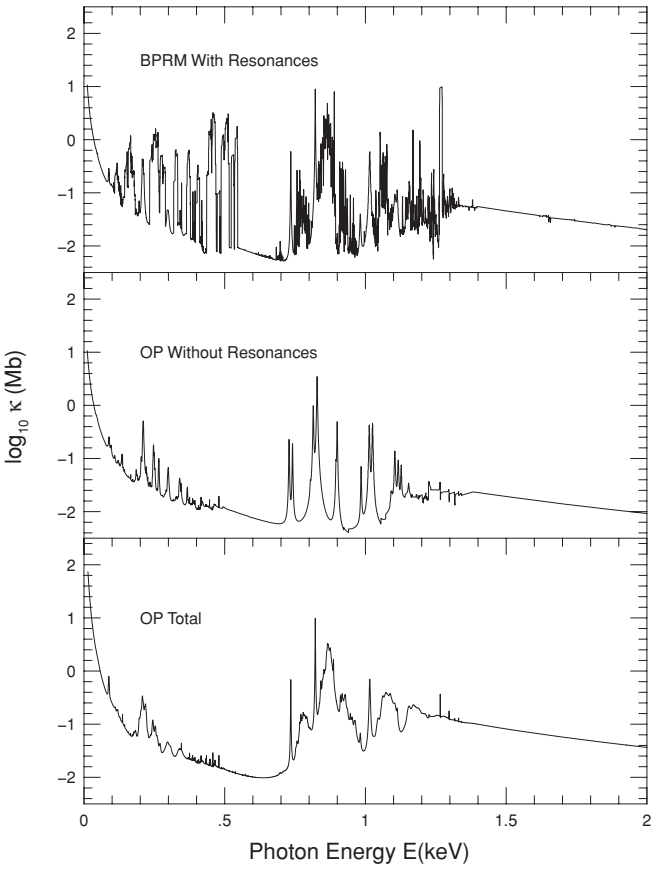

FIG. 5. Partial monochromatic opacity of Fe XVII: $\log_{10}\kappa$ (Mb) at temperature $T = 2.24 \times 10^6$ K and electron density $N_e = 10^{23}$ cm^{-3}, corresponding to the base of the solar convection zone where the Fe XVII ion is the largest contributor to opacity. The top panel presents results using BPRM bound-free cross sections with resonances computed in this work and the middle panel shows the same but without resonances using earlier data from the Opacity Project (OP). Identical datasets from OP are employed for the bound-bound transitions; therefore, the differences are mainly due to the resonances included in the present work. For comparison, the bottom panel shows total OP opacities [36] that include core-excitation resonances as lines, with autoionization widths considered perturbatively as well as the high-energy K-shell continuum opacity not yet included in BPRM calculations (see text).

atomic parameters computed herein. The details of the new opacity code and results will be reported later. However, we note in passing that, since the resonances would dissolve more readily than lines, it is likely to significantly affect continuum lowering, manifest in opacity spectra, and to be highly sensitive to temperature and density. Lines dissolve and eventually merge into the continuum in the high–temperature-density regime. Then a precise accounting may not be necessary; they are often treated as "unresolved transition arrays" (UTAs) since J-J' transitions are merged together and often subsumed by line broadening [39]. However, our aim is to focus on delineation of atomic features as fully as possible so that their contributions to opacity in different temperature-density regimes can be accurately ascertained.

The BPRM opacity cross sections in Fig. 5 are compared with two other sets of results from OP. Although over 20 000 oscillator strengths for bound-bound transitions are also computed, we use exactly the same data for lines as the earlier OP calculations described in [2]. Thus, the differences between the the 60CC BPRM results from the present work in the upper panel of Fig. 5 and the limited OP without resonances in the middle panel are entirely due to the differences in the bound-free datasets. The opacity calculations are done at a temperature-density representative of plasma conditions at the base of the solar convection zone: $\log_{10} T(\mathrm{K}) = 6.35$ and $\log_{10} N_e = 23$. These parameters also lie in the range currently under investigation in the Z-pinch plasmas for measurement of transmission spectra [1]. In addition to resonance contributions, there are some other differences. The OP data include cross sections extrapolated out to very high energies, ~500 Ry. The BPRM data have also been processed to include these high-energy "tails," but the form is slightly different. The background opacity is important to obtain a value for RMOs that spans over 4 decades in temperature, $\log_{10} T(\mathrm{K}) = 3.5$ to 7.5.

Calculations for the monochromatic opacity κ_ν are carried out for each ion along isotherms in $\log_{10} T$ for a range of electron densities $\log_{10} N_e$. The Rosseland Mean Opacity (RMO) κ_R is defined in terms of κ_ν as

$$\frac{1}{\kappa_R} = \frac{\int_0^\infty g(u)\frac{1}{\kappa_\nu}du}{\int_0^\infty g(u)du}, \quad g(u) = u^4 e^{-u}(1-e^{-u})^{-2}, \quad (10)$$

where $g(u)$ is the Planck weighting function (corrected for stimulated emission). The quantity κ_ν is primarily a function of the oscillator strengths f, photoionization cross sections σ_ν, level populations N_i, and line profile factor ϕ_ν:

$$\kappa_\nu^{bb}(i \to j) = \left(\frac{\pi e^2}{m_e c}\right) N_i f_{ij} \phi_\nu, \quad \kappa_\nu^{bf} = N_i \sigma_\nu. \quad (11)$$

Whereas further code developments are required to include all opacity contributions, we already find large enhancements in κ_R due to resonances, primarily from the $n = 3$ complex. The resonance contribution is included in existing opacity codes as inner-shell bound-bound transitions [40]. The BPRM value of κ_R, also including the bound-bound oscillator strengths computed in this work (as opposed to OP), yields a value of 223.8 cm^2/g. Using the same bound-bound data as OP, the BPRM κ value is still 200.3 cm^2/g, compared to the OP value of 109.7 cm^2/g (Fig. 5). The bottom panel in Fig. 5 is the total monochromatic opacity spectrum of Fe XVII from the OP, including all contributions, with the total RMO $\kappa_R = 306.9\ \mathrm{cm}^2/\mathrm{g}$. Thus the BPRM value using the data computed in this work is 27% lower. This is primarily because of two factors: (i) The high-energy "tails" are made more precise with even more-extended BPRM calculations that include the K-ionization thresholds, which would attenuate the bound-free opacity in the large energy range between the L and K levels. Although the K-shell opacity is not too significant, the K-shell resonances would thereby be included. (ii) The bound-bound oscillator strengths are computed up to $n = 10$. Therefore, there is a relatively small gap in cross sections in the region between $n = 10$ to ∞, below the photoionization thresholds of the 454 bound levels. In the earlier OP work, we began the tabulation of cross sections at $E = -z^2/\nu^2$ ($\nu \sim 10$) below each threshold. Employing a similar approximation increases the BPRM RMO value from 223.8 to 260.7 cm^2/g, to within 20% of the total OP RMO. Owing to the significance of (i) and (ii), we plan to carry out more extensive calculations than in earlier works as well to investigate if higher-n resonance complexes with $n = 4$ or 5 might be needed.

E. Unified electron-ion recombination

One of the important characteristics of PEC resonances is that they entail excited states with valence electrons that are weakly bound to the core ion. Therefore, during core excitation the outer electron remains essentially a "spectator" temporarily attached to the excited core level, and it autoionizes as that level decays to the ground state. The analogy and connection between the PEC resonances and the dielectronic recombination process is well known [21,22,31]. It is expected that the total electron-ion recombination rates of Fe XVII will also be commensurately enhanced by inclusion of the PEC resonances via detailed balance (Milne relation; see, e.g., [22,31]).

A major application of the computed cross sections is in benchmarking total unified recombination rate coefficients, including radiative and dielectronic recombination, for Fe XVII at high temperatures, including those where Fe XVII is abundant in coronal plasmas, such as in the solar corona and solar flares, up to at least 10^7 K. That is possible because we have considered a large energy range up to the excitation of $n = 3$ levels of the recombining ion Fe XVIII. Towards that end, we have also repeated the entire photoionization calculation to obtain partial cross sections for the 454 bound levels of Fe XVII with the residual ion in the ground state alone.

V. CONCLUSION

In this report we have presented results from a pilot project of complete BPRM calculations for photoionization of an atomic system, Fe XVII, larger than a He- or Li-like ion, ($h\nu$ + Fe XVII → e+ Fe XVIII). The aim was to study in detail the extent and range of high-energy resonances of importance in practical applications. The BPRM calculations consider all fine structure levels up to $n(SLJ) \leqslant 10$, with spectroscopic identification. In addition to photoionization cross sections, the bound-bound oscillator strengths for transitions among the 454 computed levels of Fe XVII are also being computed. These

datasets of atomic parameters should be of unprecedented accuracy and be generally useful.

The comprehensive calculations were carried out so as to compare with the erstwhile OP calculations that treated resonances as lines. A clear distinction is made between pure bound-bound transitions and bound-free transitions into autoionizing levels. The results from this work demonstrate that opacities may be computed using BPRM cross sections and transition probabilities, and it is likely that plasma opacities in general, and those of Fe ions in particular, would be different from earlier opacities using atomic cross sections that accurately consider the energy distribution of resonances.

Monochromatic opacities of Fe XVII are computed and compared with the OP work. These are not the final opacities, and some further developments are still necessary, such as resonance-broadening mechanisms and K-shell contributions. Nevertheless, we are able to compute complete BPRM radiative datasets and Rosseland mean opacities that are sufficiently close to OP values to imply that future calculations of plasma opacities can be carried out with higher precision.

Three other applications of the present work might be pointed out. (i) Accurate unified electron-ion recombination rate coefficients can be calculated. (ii) Benchmarking may be done of experimental measurements of absolute photoionization cross sections on accelerator-based light sources, which are now being made for multiply charged Fe ions (see, e.g., [41]). It has now been established that the experimental beams contain ions not only in the ground state but also in several metastable levels. An admixture of ground state plus a few excited metastable levels is therefore necessary to benchmark experimental measurements against theory. In addition, the experimental measurements are capable of reaching energies where PEC resonances occur (see, e.g., [42]). (iii) The radiative data for Fe XVII should be useful for x-ray spectral diagnostics and NLTE models (Ref. [43] presents a detailed Grotrian diagram of Fe XVII levels up to $n = 4$).

Estimates of uncertainties in the large sets of parameters reported in this paper, as well as that required in future calculations of opacities, are as follows: The accuracy of the 454 theoretically computed energy levels has been ascertained in the text by comparison with experimentally observed levels; in general better than 1%. The differences between BPRM cross sections and measurements for photoionization and recombination for Fe XVII are found to be within experimental uncertainties of ∼10% to 20% [25]. Similarly, most of the strong transitions in the extensive dataset of Fe XVII oscillator strengths should be better than 10% accurate [35]. The present calculations for photoionization employ a much larger 60CC eigenfunction expansion than the 3CC calculations in previous studies [25,35], and are expected to be more accurate. Uncertainties in the BPRM monochromatic opacities should be commensurate with those in the underlying 60CC data. However, the final accuracy of derived mean Rosseland and Planck opacity ions is as yet undetermined since photoionization cross sections extrapolated or computed at high energies are to be included for all 454 bound states. The problem is further complicated since the aim is to obtain statistical averages with sampled opacities (albeit on a finer mesh of 10^5 frequencies as opposed to 10^4 in earlier calculations) that would approach the accuracy (∼1%) needed to improve over existing uncertainties of ∼5% [20].

Electronic files for photoionization cross sections, energy levels, and oscillator strengths are available electronically from the NORAD website [34].

ACKNOWLEDGMENTS

This work was partially supported by the NASA Astronomy and Physics Research Analysis Program (SNN) and the US Department of Energy (AKP). The computational work was carried out at the Ohio Supercomputer Center in Columbus Ohio.

[1] J. E. Bailey *et al.*, Phys. Plasmas **16**, 058101 (2009).
[2] M. J. Seaton, Y. Yan, D. Mihalas, and A. K. Pradhan, Mon. Not. R. Astron. Soc. **266**, 805 (1994).
[3] The Opacity Project Team, *The Opacity Project* (Institute of Physics Publishing), Vol. 1 (1995), Vol. 2 (1996).
[4] F. J. Rogers and C. A. Iglesias, *The Opacity Project*, Vol. 1 (Institute of Physics Publishing, 1995).
[5] D. Grupe, S. Komossa, L. C. Gallo, A. C. Fabian, J. Larsoon, A. K. Pradhan, and D. Xu, Astrophys. J. **681**, 982 (2008).
[6] D. Mihalas, *Stellar Atmospheres* (Freeman, 1978).
[7] S. N. Nahar and A. K. Pradhan, **Rad. Proc. Phys. Chem. 70**, 323 (2004).
[8] D. G. Hummer, K. A. Berrington, W. Eissner, A. K. Pradhan, H. E. Saraph, and J. A. Tully, Astron. Astrophys. **279**, 298 (1993).
[9] P. G. Burke and W. D. Robb, Adv. At. Mol. Phys. **11**, 143 (1975).
[10] P. G. Burke, A. Hibert, and D. Robb, J. Phys. B **4**, 153 (1971).
[11] P. G. Burke and K. A. Berrington, *Atomic and Molecular Processes: An R-Matrix Approach* (Institute of Physics Publishing, Bristol, 1993).
[12] N. S. Scott and K. T. Taylor, Comput. Phys. Commun. **25**, 347 (1982).
[13] K. A. Berrington, W. B. Eissner, and P. H. Norrington, Comput. Phys. Commun. **92**, 290 (1995).
[14] S. N. Nahar and A. K. Pradhan, Astrophys. J. Suppl. **162**, 417 (2006).
[15] M. Asplund, N. Grevesse, J. Sauval, and P. Scott, Annu. Rev. Astron. Astrophys. **47**, 481 (2009).
[16] A. K. Pradhan and S. N. Nahar, *Recent Directions Astrophysical Quantitative Spectroscopy and Radiation Hydrodynamics*, AIP Press **1171**, 52 (2009).
[17] S. Basu and H. N. Antia, Phys. Rep. **457**, 217 (2008).
[18] F. Delahaye and M. Pinsonneault, Astrophys. J. **649**, 529 (2006).
[19] J. N. Bahcall, S. Basu, M. Pinsonneault, and A. M. Serenelli, Astrophys. J. **618**, 1049 (2005).

[20] M. J. Seaton and N. R. Badnell, Mon. Not. R. Astron. Soc. **354**, 457 (2004).
[21] Y. Yu and M. J. Seaton, J. Phys. B **20**, 6409 (1987).
[22] A. K. Pradhan and S. N. Nahar, *Atomic Astrophysics and Spectroscopy* (Cambridge University Press, 2011).
[23] M. P. Scott, see [36].
[24] A. K. Pradhan, S. N. Nahar, and H. L. Zhang, Astrophys. J. Lett. **549**, L265 (2001).
[25] H. L. Zhang, S. N. Nahar, and A. K. Pradhan, Phys. Rev. A **64**, 032719 (2001).
[26] S. N. Nahar, M. Montenegro, W. Eissner, and A. K. Pradhan, Phys. Rev. A **82**, 065401 (2010).
[27] W. Eissner, M. Jones, and N. Nussbaumer, Comput. Phys. Commun. **8**, 270 (1974).
[28] D. Mihalas, D. G. Hummer, and W. Däppen, Astrophys. J. **331**, 815 (1988).
[29] J. Sugar and C. Corliss, Elements: Potassium through Nickel. J. Phys. Chem. Ref. Data **14**, Suppl. No. 2 (1985), listed in NIST compiled website [http://physics.nist.gov/cgi-bin/AtData/main_asd].
[30] S. N. Nahar and A. K. Pradhan, Phys. Scr. **61**, 675 (2000).
[31] S. N. Nahar and A. K. Pradhan, Phys. Rev. A **49**, 1816 (1994).
[32] S. N. Nahar, J. Quantum Spectrosc. Radiat. Transfer **109**, 2417 (2008).
[33] M. J. Seaton, J. Phys. B **20**, 6363 (1987).
[34] [www.astronomy.ohio-state.edu/∼nahar/nahar_radiativeatomic-data].
[35] S. N. Nahar, W. Eissner, G.-X. Chen, and A. K. Pradhan, Astron. Astrophys. **408**, 789 (2003).
[36] C. Mendoza *et al.*, Mon. Not. R. Astron. Soc. **378**, 1031 (2007).
[37] S. N. Nahar and A. K. Pradhan, Phys. Rev. A **44**, 2935 (1991).
[38] S. N. Nahar, A. K. Pradhan, and H. L. Zhang, Phys. Rev. A **63**, 060701 (2001).
[39] B. F. Rozsnyai, S. D. Bloom, and D. A. Resler, Phys. Rev. A **44**, 6791 (1991).
[40] Opacity sources do not usually report monochromatic opacity spectra for individual ions (viz. [36]). Code development is under way to isolate different opacity contributions in the OP work to provide detailed comparisons with improved opacities using the BPRM data exemplified by the pilot calculations presented herein.
[41] N. El Hassan, J. M. Bizau, C. Blancard, P. Cosse, D. Cubaynes, G. Faussurier, and F. Folkmann, Phys. Rev. A **79**, 033415 (2009).
[42] M. Habibi, D. A. Esteves, R. A. Phaneuf, A. L. D. Kilcoyne, A. A. Aguilar, and C. Cisneros, Phys. Rev. A **80**, 033407 (2009).
[43] G. X. -Chen, A. K. Pradhan, and W. B. Eissner, J. Phys. B **36**, 453 (2003).